JOURNAL OF APPLIED ELECTROCHEMISTRY 25 (1995) 543–555

Mass transport effects on the electrodeposition of iron–nickel alloys at the presence of additives

K.-M. YIN, J.-H. WEI, J.-R. FU

Department of Chemical Engineering, Yuan-Ze Institute of Technology, Neili, Taoyuan 32026, Taiwan

B. N. POPOV, S. N. POPOVA, R. E. WHITE

Department of Chemical Engineering, University of South Carolina, South Carolina 29208, USA

Received 10 May 1994; revised 20 September 1994

Iron–nickel (Fe–Ni) plating bath solution chemistry was studied by determining the Fe–Ni equilibrium concentrations at various pH levels. It was found that the alloy composition is determined by solution equilibria, mass transfer of the electroactive species within the diffusion layer and by the surface coverage of the additives on the electrode. The effect of the rotation speed of the disc electrode and the presence of organic additives on the deposition of Fe–Ni alloys are evaluated. Boric acid increases the absolute iron deposition rate, while it inhibits the rate of nickel reduction. Saccharin and ethylene diamine influence the metal deposition rate but are not as effective as boric acid.

List of symbols

c_j concentration of species j ($mol\,cm^{-3}$)
$c_{j,s}$ concentration of species j at interface ($mol\,cm^{-3}$)
E_{appl} applied potential (V)
F Faraday constant ($96\,487\,C\,mol^{-1}$)
k_M rate constant for the deposition of M ($mol\,cm^{-2}\,s^{-1}$)
K_j stability constant of species j ($mol^{-1}\,cm^3$)
$K_{j,ads}$ adsorption constant of species j ($mol\,cm^{-3}$)
n_M number of electron transferred for metal deposition
r_M deposition rate of M ($mol\,cm^{-2}\,s^{-1}$)
R gas constant ($8.314\,J\,mol^{-1}\,K^{-1}$)
T absolute temperature (K)

Greek symbols

α_M transfer coefficient for the deposition of M (dimensionless)
θ_{empty} uncovered surface fraction, dimensionless
θ_j surface coverage fraction of species j, (dimensionless)

1. Introduction

Iron–nickel (Fe–Ni) electrodeposition is a simple, one-step process for the production of magnetic films used in electronic applications. The plating technique attracts industrial application because of its low cost and its capability for deposition on almost any geometry [1]. However, explanations of the deposition mechanism are diverse. Dahms and Croll [2, 3] found that Fe–Ni codeposition appears closely related to the local pH rise at the interface due to the hydrogen evolution reaction. According to these authors, the preferential precipitation of iron hydroxide compared to nickel hydroxide causes the inhibition of nickel deposition but iron discharges through the iron hydroxide film. Romankiw [4] revised the Dahms and Croll mechanism suggesting that a trace amount of Fe^{3+} in the solution causes precipitation of $Fe(OH)_3$, and that such a film accounts for the selective discharge. Nichol and Philip [5] attributed the underpotential deposition to the appearance of an iron dominant intermetallic compound. Andricacos *et al.* [6, 7] used a rotating ring-disc electrode and a rotating-disc electrode to study Fe–Ni deposition. They found that iron deposition is under mass transfer limitation, while nickel deposition is kinetically controlled. Talbot *et al.* [8, 9] and Hessami and Tobias [10] proposed that the charge transfer of $Fe(OH)^+$ and $Ni(OH)^+$ species is responsible for anomalous codeposition of Fe–Ni alloys. According to these authors higher $Fe(OH)^+$ concentration, compared to $Ni(OH)^+$, causes the higher iron plating rate. The importance of metal hydroxide ions in the iron–nickel plating system was suggested by Bockris *et al.* [11] and Matulis and Slizys [12] on the single metal species deposition. They suggested that the reduction of adsorbed metal hydroxide ion is the rate determining step for the metal deposition. Matlosz [13] proposed a model in which the competitive surface adsorption of Ni(I) and Fe(I) intermediates determine their respective deposition rates and alloy deposition. We used galvanostatic pulse and pulse reverse and potentiostatic pulse techniques to study the plating of Fe–Ni alloys in the presence of organic additives [14, 15]. Electrodeposition of the alloy was explained by the

0021-891X

concentration depletion of reactants and the surface coverage of the additives on the electrode.

The objective of this work was to explain the codeposition of iron–nickel alloys in the presence of organic additives through a mechanism which takes into account Fe–Ni plating bath solution chemistry, mass transfer and electrode surface reactions.

2. Experimental details

Four different plating baths were used to deposit Fe–Ni alloys. A basic plating solution (bath I) contained 0.5 M nickel sulfate, 0.1 M iron sulfate and 0.5 M sodium sulfate as a supporting electrolyte. The second plating solution (bath II) was a traditional Watts nickel plating bath with the addition of ferrous ions (i.e., bath I + 0.4 M boric acid). Bath III contained bath II + 0.4 M ethylene diamine and bath IV contained bath II + 0.01 M sodium saccharin. The Fe–Ni plating bath pHs were adjusted to 3 by using 20% H_2SO_4. 200 ml of plating solution was held in a glass cell with an outer jacket convenient to water circulation. Although each plating was carried out in a freshly prepared solution, no deaeration was done before plating. The temperature was maintained at 25° C by a circulator. The solution mass transfer was controlled by a rotator (EG&G RDE 616). Self-designed exchangeable copper disc with an exposed area of 0.458 cm^2 was connected to the shaft of the rotator as the working electrodes. Special care was taken to prevent leaks by using a Teflon seal between the copper disc and casing. Platinum wire was used as the anode. Before plating, the copper discs were polished with 0.3 μm and 0.05 μm aluminium powder, followed by surface activation in 20% H_2SO_4 solution. The deposition potential was controlled by a Potentiostat/Galvanostat (EG&G M263) using a saturated calomel electrode (SCE) as a reference electrode. The deposition time was adjusted so that the total charges applied were about four coulombs. The deposited alloys were dissolved in acids, then diluted and nickel and iron contents in the alloy were determined using a GBC 902 atomic absorption spectrometer. The side reaction of hydrogen evolution was determined by subtracting the partial current of nickel and iron from the total current.

SEM and EDS were used for the study of Fe–Ni surface morphologies and element distributions at different applied potentials.

3. Results and discussion

3.1. *Solution chemistry of Fe–Ni plating bath*

The solution chemistry was studied by determining the Fe–Ni plating bath equilibrium concentrations at various pH levels. The concentration of all electroactive species in the bath were calculated by using various element balances, equilibrium conditions, and the electroneutrality condition for a specified pH. In order to obtain the whole spectrum as a function of pH, suitable amounts of NaOH and H_2SO_4 were used in the computation. The total materials are the sum of 1000 g of H_2O + 147.35 g (0.5 M) $NiSO_4$ + 13.89 g (0.05 M) $FeSO_4$ + 125 g (0.5 M) Na_2SO_4.

The governing equations for different regions and the computational details are summarized and shown in the appendix. The equations were solved by using the Newton–Raphson iterative method. Evaluated solution equilibrium concentrations as a function of pH are presented in Fig. 1 where three regions are considered. In the first region all electroactive

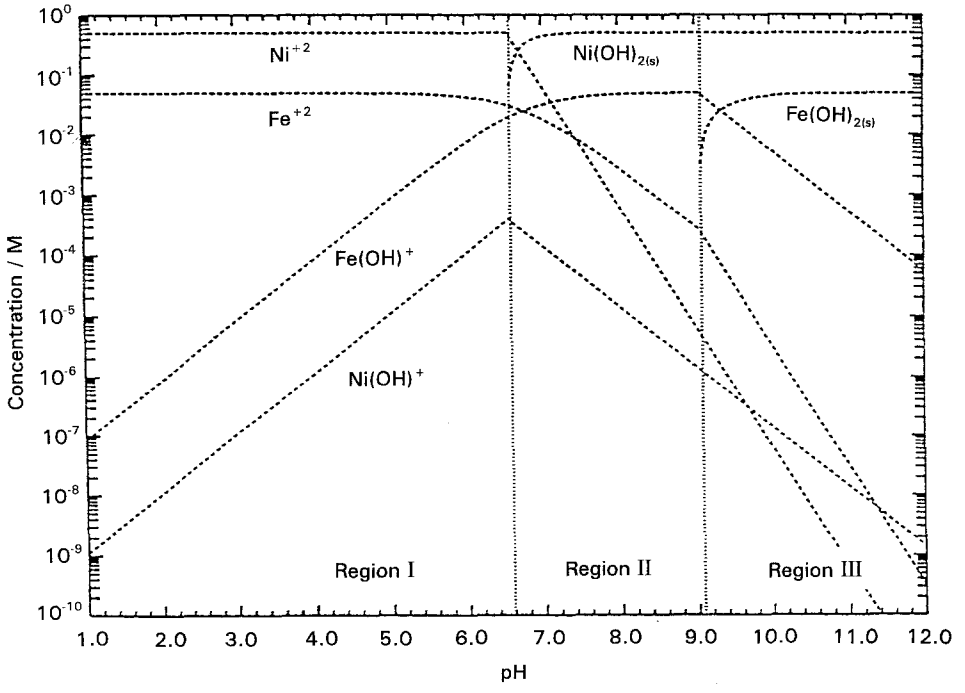

Fig. 1. Solution equilibrium concentrations in Fe–Ni plating bath as a function of pH.

species are completely dissolved. In the second region, $Ni(OH)_2$ precipitates at a higher pH, while no $Fe(OH)_2$ precipitation occurs. In the third region both $Ni(OH)_2$ and $Fe(OH)_2$ precipitations occur at high pH levels. At pH < 6.6, there was no precipitation of any of the species present in the electrolyte. Also, according to Fig. 1, $Ni(OH)_2$ precipitates preferentially instead of $Fe(OH)_2$. Because of the difference in metal hydroxide ion stability constants ($K_{sp,Ni(OH)_2} = 6.3 \times 10^{-16}$ mol^3 L^{-3}; $K_{sp,Fe(OH)_2} = 3.16 \times 10^{-14}$ mol^3 L^{-3}), $Ni(OH)_2$ precipitation occurs at a pH two units smaller than $Fe(OH)_2$. These results were not consistent with the Dahms and Croll theory [2, 3]. They suggested that the preferential adsorption of $Fe(OH)_2$ rather than $Ni(OH)_2$ occurs on the electrode at high pH values. To support the preferential adsorption of $Fe(OH)_2$, it must be assumed that both $Fe(OH)_2$ and $Ni(OH)_2$ are in the form of colloids and have different adsorption rates; this is an unreasonable assumption. Besides the fact that Ni^{2+} ions are present in the electrolyte in much higher concentration than Fe^{2+}, according to Fig. 1, the $Fe(OH)^+$ concentration is two orders of magnitude larger than the $Ni(OH)^+$ concentration. From the shape of the equilibrium curves in Fig. 1, it can also be concluded that any metal hydroxide will precipitate completely due to a small change in pH. Thus, a small change in pH at the electrode surface should have dramatic effects on alloy composition and surface morphology. Although Fig. 1 illustrates equilibrium conditions, it serves as a guide for solution behaviour of the electroactive species in an Fe–Ni codeposition process.

3.2. *Mass transfer effects on the electrodeposition of iron–nickel alloys*

Nickel, hydrogen and iron partial current densities obtained in bath I containing 0.5 M $NiSO_4$, 0.1 M $FeSO_4$ and 0.5 M Na_2SO_4 are shown in Figs 2, 3 and 4, respectively. In Fig. 2, a higher nickel reduction rate corresponds to a larger applied potential. However, the reduction rate decreases as the electrode rotation speed is increased. Similar results were obtained by Andricacos *et al.* [6] in a chloride bath (0.2 M $NiCl_2$, 0.005 M $FeCl_2$, 0.4 M boric acid, and 0.5 M NaCl). They found that the inhibition of nickel reduction occurs only in the region where iron reduction is under mass transfer control and depends upon the flux of Fe^{2+} to the electrode surface. However, as shown in Figs 2 and 4, the inhibition of nickel occurs even at small overvoltages where iron is not in the mass transfer controlled region. The anomalous behaviour observed at higher rotation speed can be explained by taking into account the effect of pH on the surface concentration of the electroactive species $Ni(OH)^+_{ads}$ [12] and by competition of $Ni(OH)^+_{ads}$ with $Fe(OH)^+_{ads}$ for the surface active sites [13]. According to the mechanism of single nickel plating [12], an adsorbed surface

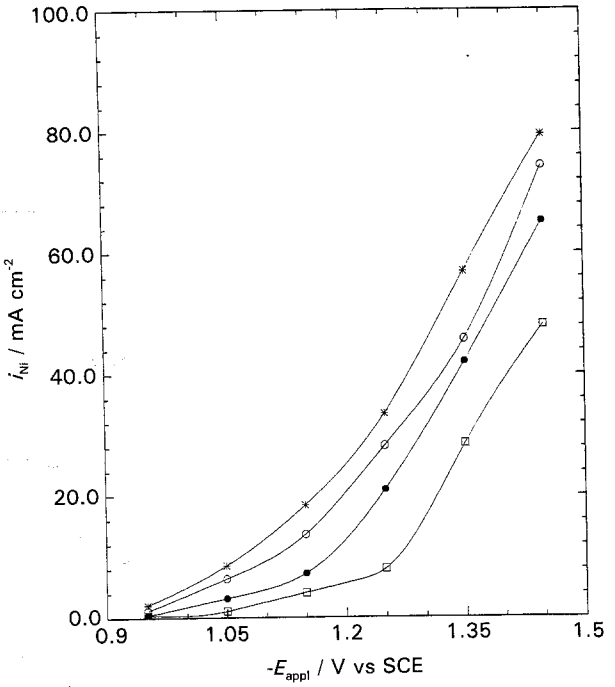

Fig. 2. Effect of electrode rotation speed on nickel partial current density in bath I containing: 0.5 M $NiSO_4$, 0.1 M $FeSO_4$ and 0.5 M Na_2SO_4, pH 3. Key: (*) 500 rpm, (○) 1000 rpm, (●) 2000 rpm, (□) 3000 rpm.

intermediate, $Ni(OH)^+$, participates in the nickel electrodeposition process:

$$Ni^{2+} + OH^- \longleftrightarrow Ni(OH)^+ \quad (1)$$

$$Ni(OH)^+_{ads} + 2e^- \longrightarrow Ni + OH^- \quad (2)$$

Since the hydrogen evolution rate (h.e.r.) is mass transfer controlled, the rise of interfacial pH due to h.e.r. is expected to be larger at lower rotation speed. The rise of surface pH favours the formation

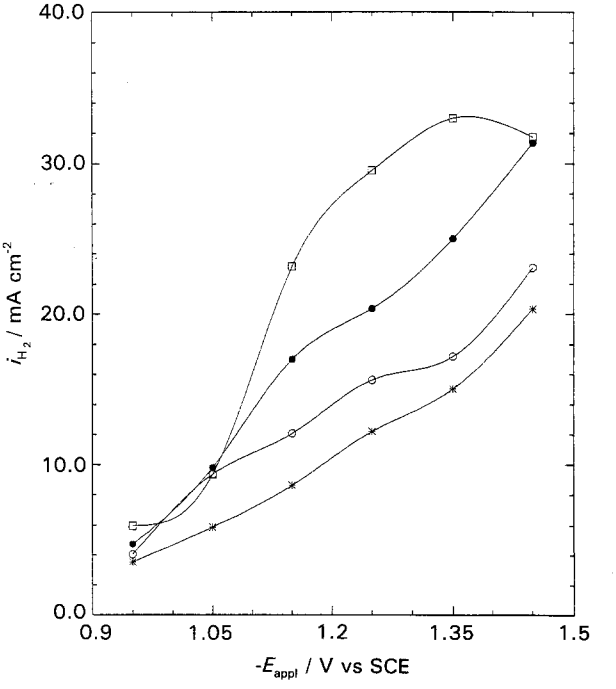

Fig. 3. Effect of electrode rotation speed on hydrogen partial current density in bath I containing: 0.5 M $NiSO_4$, 0.1 M $FeSO_4$ and 0.5 M Na_2SO_4, pH 3. Key as in Fig. 2.

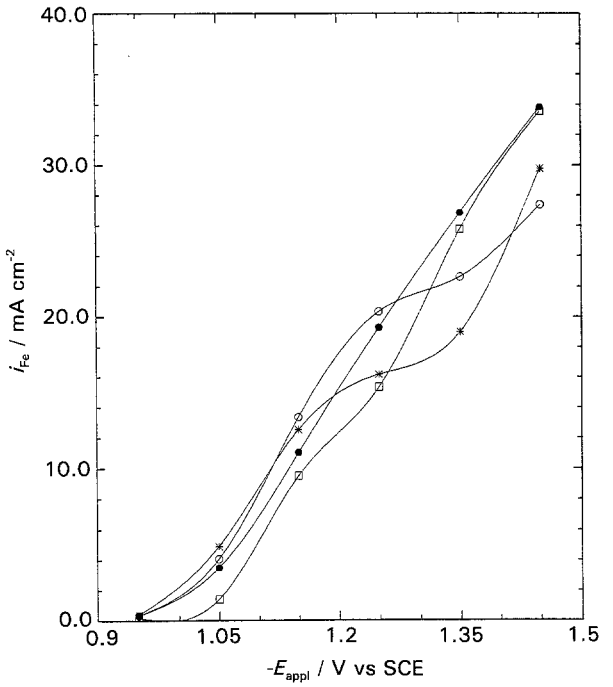

Fig. 4. Effect of electrode rotation speed on iron partial current density in bath I containing: 0.5 M $NiSO_4$, 0.1 M $FeSO_4$ and 0.5 M Na_2SO_4, pH 3. Key as in Fig. 2.

of nickel hydroxide ions within the diffusion layer which adsorb on the surface to produce nickel according to Equations 1 and 2. Also, higher rotation speed enhances the mass transfer of ferrous ions to the electrode surface and favours the surface adsorption of $Fe(OH)^+$. This effect causes an inhibition of the nickel reduction process due to the competition of $Fe(OH)^+$ with $Ni(OH)^+$ for surface active sites [13].

The dependence of the hydrogen partial current densities (i_{H_2}) on the electrode rotation speed are given in Fig. 3. Higher rotation speed in Fig. 3 favours the h.e.r., suggesting a strong mass transfer limitation for hydrogen partial current densities. The hydrogen evolution reaction, which occurs at the interface, can be expressed as

$$2H^+ + 2e^- \longrightarrow H_2 \quad (3)$$

$$2H_2O + 2e^- \longrightarrow H_2 + 2OH^- \quad (4)$$

According to the Levich equation [16], the limiting current density for hydrogen evolution in Equation 3 depends on the electrode rotation speed and is 2.0 and 4.9 mA cm^{-2} for $w = 500$ and $w = 3000$ rpm, respectively. More protons can also be released at the interface from water dissociation which in turn may enhance the hydrogen evolution reaction in Equation 3. However, water dissociation cannot account for the observed h.e.r., indicating that water reduction in Equation 4 dominates the hydrogen generation process. Increasing the overvoltage causes both reactions to induce an increase in pH at the interface. As shown in Fig. 3, higher electrode rotation speed enhances the hydrogen ion transfer from the bulk and reduces the accumulation of OH^- at the interface. In other words, higher electrode rotation maintains a low pH at the interface for a fixed applied potential, a condition which favours h.e.r.

The effect of the electrode rotation speed on the iron partial current densities (i_{Fe}) is given in Fig. 4. Two potential regions can be observed. In the low potential region, higher electrode rotation speed results in a lower iron partial current density (i_{Fe}), while in the high potential region, an increase in mass transfer enhances i_{Fe}. This can be explained taking into account the mechanism of single iron plating [11]

$$Fe^{2+} + OH^- \longleftrightarrow Fe(OH)^+ \quad (5)$$

$$Fe(OH)^+_{ads} + 2e^- \longrightarrow Fe \quad (6)$$

Similar to nickel electrodeposition, at low overvoltages, higher electrode rotation speed induces a lower pH at the interface, which is not favourable for the production of $Fe(OH)^+$ in the electrolyte. As a consequence, lower i_{Fe} is expected when the electrode rotation speed increases. At high overvoltages $Fe(OH)^+$ is easily consumed at the interface and the mass transfer of Fe^{2+} ions from the bulk of the electrolyte to the surface becomes the limiting factor for iron electrodeposition. At the electrode interface, the ferrous ion undergoes instantaneous homogeneous reaction, (see Equation 5) to produce $Fe(OH)^+$ which is further reduced to iron according to Equation 6. In Fig. 4, the intersection between the two sequential iron partial current density curves occurs at higher current densities as the rotation speed increases, indicating, again, the influence of mass transfer control on iron deposition.

According to Bockris *et al.* [11] and Matulis *et al.* [12], iron and nickel electrodeposition involves the adsorbate intermediates $Fe(OH)^+$ and $Ni(OH)^+$, respectively. To understand the mechanism of Fe–Ni alloy deposition, it is of interest to investigate the competition between both species in alloy electrodeposition. By comparing the partial current densities of pure metal deposition with those when both metals are present in the solution valuable information can be obtained about the interactions between the deposition processes and deposited metals. Partial current densities of single nickel electrodeposition from electrolyte containing 0.5 M $NiSO_4$ and 0.5 M Na_2SO_4 are shown in Fig. 5. An unexpected maximum of nickel partial current density is observed for each electrode rotation speed. Higher electrode rotations induce larger peaks which are shifted to higher cathodic overpotentials. This can be explained by taking into account the changes in pH at the interface. In fact, as shown in Fig. 1, $Ni(OH)_2$ precipitates at higher interfacial pH and passivates the substrate for further nickel reduction. Thus, increasing the electrode rotation speed causes the formation of $Ni(OH)_2$ film to shift towards higher overpotentials, a phenomenon observed in Fig. 5, which results in higher i_{Ni}. In Fig. 5 before

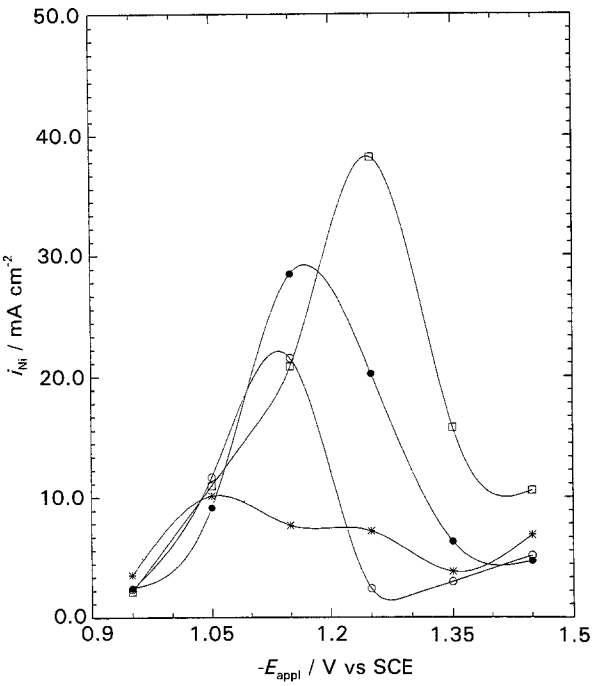

Fig. 5. Effect of electrode rotation speed on nickel partial current density in electrolyte containing: 0.5 M $NiSO_4$ and 0.5 M Na_2SO_4, pH 3. Key as in Fig. 2.

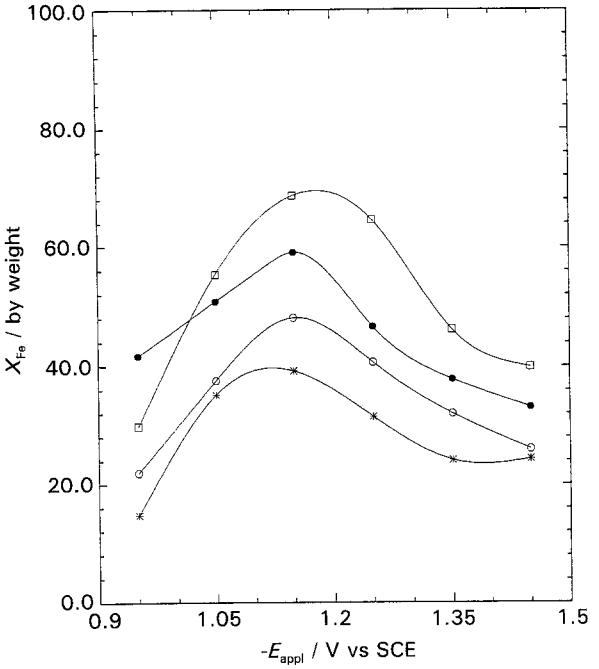

Fig. 6. Effect of electrode rotation speed on weight percentage of iron in the deposit. The deposition was carried out in bath I containing: 0.5 M $NiSO_4$, 0.1 M $FeSO_4$ and 0.5 M Na_2SO_4, pH 3. Key as in Fig. 2.

passivation occurs, nickel partial current densities, estimated for each electrode rotation speed, are higher than i_{Ni} in the alloy plating bath shown in Fig. 2. It is obvious that inhibition of the nickel reduction rate occurs due to the introduction of ferrous ions to the electrolyte. According to Matlosz's theoretical model [13], the adsorbed $Fe(OH)^+$ reduces the active sites for $Ni(OH)^+$ adsorption. However, as shown in Fig. 2, the introduction of ferrous ion can also stabilize nickel ion from precipitation. The stability constants for Equation 1 and Equation 5 are 2.2×10^4 and 1.7×10^7 M^{-1}, respectively [10]. Also, as shown in Fig. 1, the ferrous ion has a larger buffer capacity than the nickel ion. The solution equilibrium–pH dependence of the Fe–Ni plating bath presented in Fig. 1 indicates a larger buffer capacity of $Fe(OH)^+$ when compared with $Ni(OH)^+$. Thus, in the presence of ferrous ions, a lower pH can be preserved at the interface in Fe–Ni alloy plating. In other words, the presence of $Fe(OH)^+$ reduces the possibility of the occurrence of $Ni(OH)_2$, in agreement with observations in Fig. 1.

In Fig. 6, the weight percentages of iron in the alloy estimated for different electrode rotations are presented as a function of applied potential. The electrodeposition was carried out in the same electrolyte as in Fig. 2. As seen in Fig. 6, typical humps appear around $E_{appl} = -1.15$ V [6, 14, 15, 17, 18]. The iron composition profiles can be explained taking into account the kinetic parameters of both electrodeposition processes. Assuming that the adsorption equilibrium

$$MOH^+, s \longleftrightarrow MOH^+_{ads} \qquad (7)$$

exists on the surface, then the surface coverage of MOH^+_{ads} can be expressed as

$$\theta_{MOH^+} = \frac{C_{MOH^+,s}\theta_{empty}}{K_{MOH^+,ads}} = K_{MOH^+}\frac{C_{M^{2+},s}C_{OH^-,s}\theta_{empty}}{K_{MOH^+,ads}} \qquad (8)$$

The second equality in Equation 8 assumes a fast equilibrium of hydrolysis of M^{2+} at the interface. The kinetic expression for both metal reductions can be approximated by the Tafel

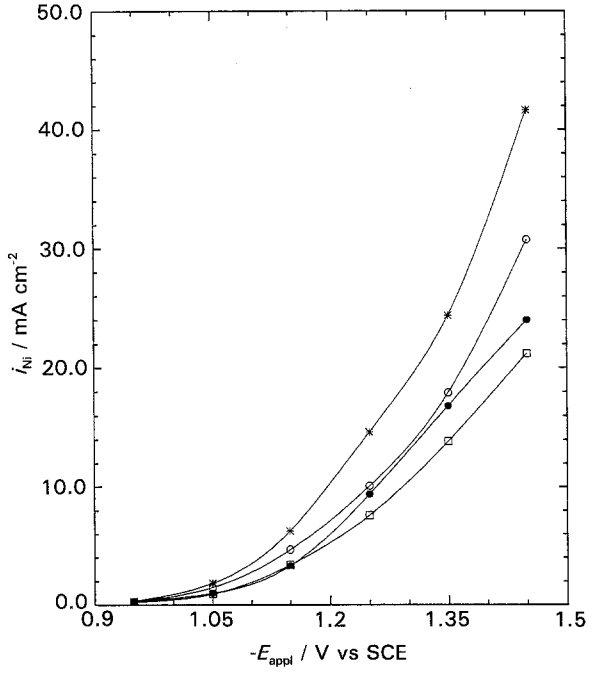

Fig. 7. Effect of electrode rotation speed on nickel partial current density in bath II containing: bath I + 0.4 M boric acid, pH 3. Key as in Fig. 2.

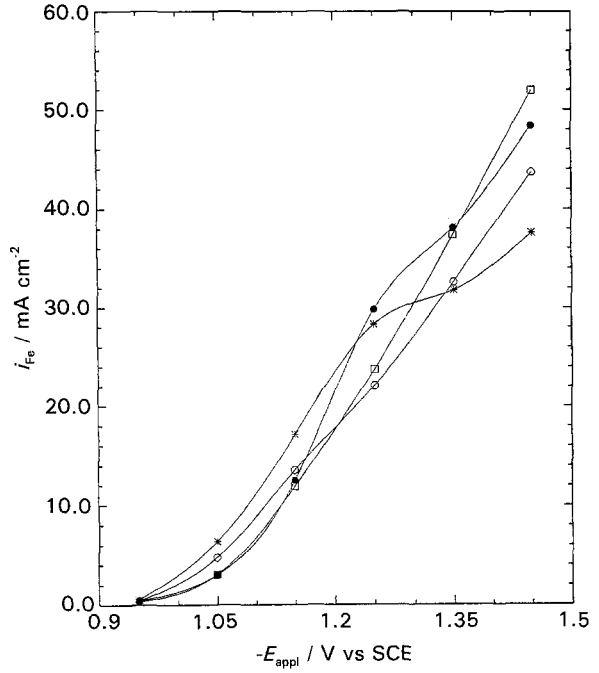

Fig. 8. Effect of electrode rotation speed on iron partial current density in bath II containing: bathI + 0.4 M boric acid, pH 3. Key as in Fig. 2.

expression:

$$r_M = k_M \theta MOH^+ \exp\left(\frac{n_M \alpha_M F(-E_{appl})}{RT}\right) \quad (9)$$

where k_M is the rate constant, n_M is the number of electrons transferred, and α_M is the kinetic transfer coefficient. The relative iron and nickel deposition rates can be derived by combining

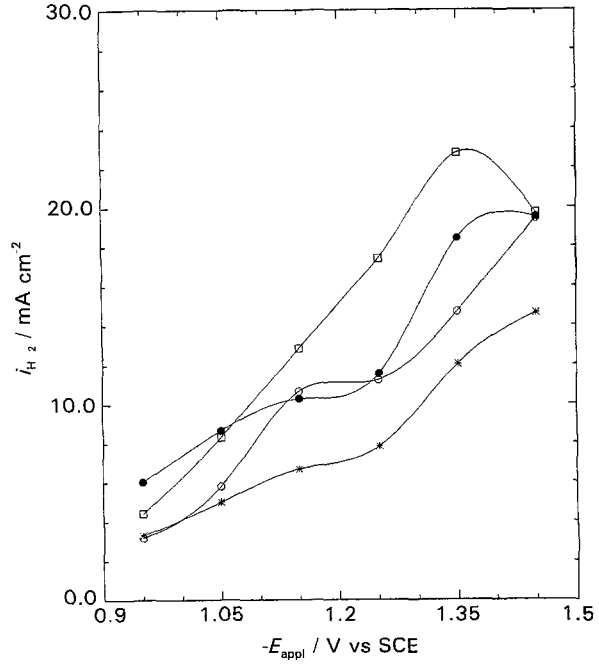

Fig. 9. Effect of electrode rotation speed on hydrogen partial current density in bath II containing: bath I + 0.4 M boric acid, pH 3. Key as in Fig. 2.

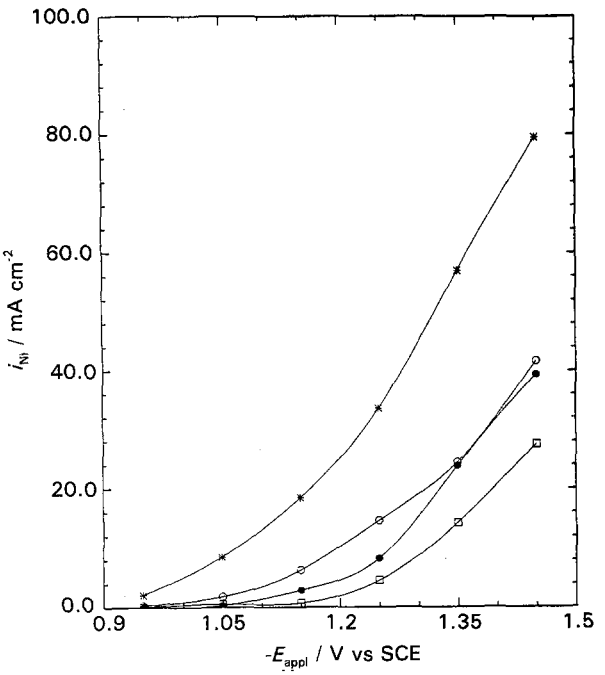

Fig. 10. Effect of various electrolytes on nickel partial current density at $w = 500$ rpm in bath I (*) containing: 0.5 M $NiSO_4$, 0.1 M $FeSO_4$, 0.5 M Na_2SO_4; bath II (○): bath I + 0.4 M boric acid, bath III (●): bath II + 0.15 M ethylene diamine; bath IV (□): bath II + 0.01 M sodium saccharin, pH 3.

Equations 8 and 9

$$\frac{r_{Fe}}{r_{Ni}} = \frac{k_{Fe} K_{Fe(OH)^+} K_{Ni(OH)^+,ads} C_{OH^-,s} C_{Fe^{2+}s}}{k_{Ni} K_{Ni(OH)^+} K_{Fe(OH)^+,ads} C_{OH^-,s} C_{Ni^{2+},s}} \times \exp\left(\frac{2(\alpha_{Fe} - \alpha_{Ni}) F(-E_{appl})}{RT}\right) \quad (10)$$

At low overpotentials, the depletion of both $C_{Fe^{2+}}$ and $C_{Ni^{2+}}$ are minor and if $\alpha_{Fe} > \alpha_{Ni}$, the deposition rate ratio in Equation 10 increases with $-E_{appl}$. According to the apparent transfer coefficients

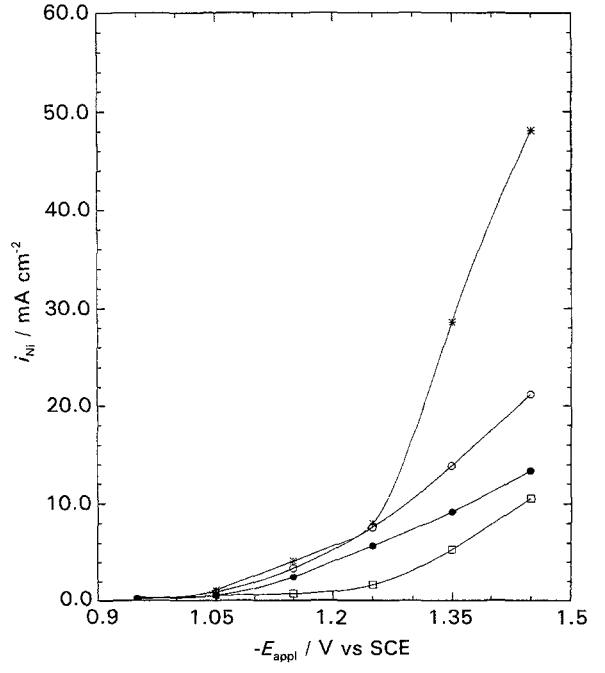

Fig. 11. Effect of various electrolytes on nickel partial current density at $w = 3000$ rpm. Key as in Fig. 10.

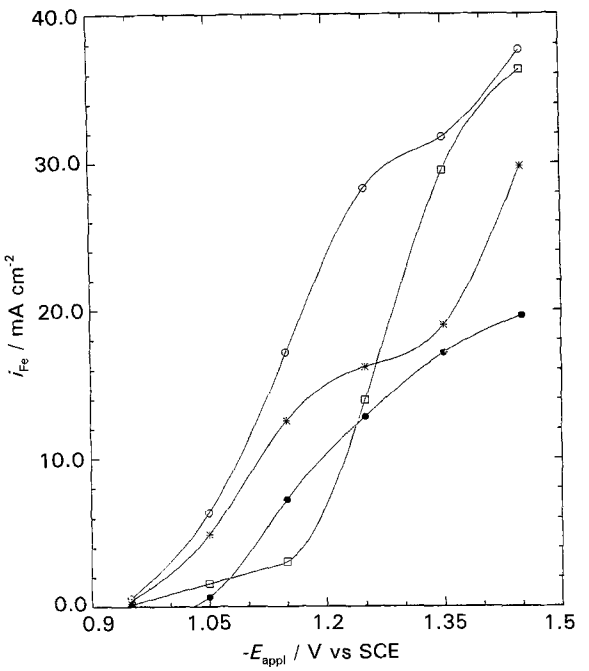

Fig. 12. Effect of various electrolytes on iron partial current density at $w = 500$ rpm. Key as in Fig. 10.

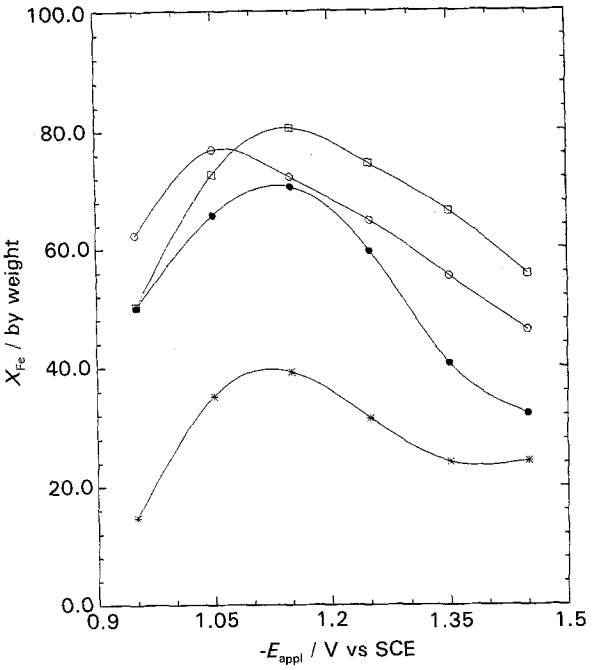

Fig. 14. Effect of different electrolytes on weight percentage of iron in the deposit. The deposition was carried out at $w = 500$ rpm. Key as in Fig. 10.

of metal depositions tabulated by Tanaka and Tamamushi [19], iron deposition has a transfer number of 0.5. The apparent transfer coefficient value on nickel deposition from sulfate solutions is in the range between 0.26 and 0.31. At high overvoltages, the depletion of $C_{Fe^{2+},s}$ is more severe than the depletion of $C_{Ni^{2+},s}$ ions, causing a decrease of r_{Fe}/r_{Ni} with $-E_{appl}$. The larger transfer coefficient for iron reduction and smaller ferrous concentration will cause the mass transfer influence for ferrous ions to occur at lower overvoltages compared with those for nickel ions. Overall, as shown in Fig. 6, at fixed potential, X_{Fe} in the deposit increases with rotation speed. Along with Fig. 6, Equation 10 reveals that at fixed potential, $C_{Fe^{2+},s}/C_{Ni^{2+},s}$ should increase as the rotation speed of the electrode increases.

The effect of various additives on i_{Ni} and i_{Fe} is shown in Figs 7–13. Partial current densities for nickel and iron electrodeposition in the presence of boric acid in the electrolyte are shown in Figs 7 and 8, respectively. In Fig. 7, the nickel reaction rate is inhibited significantly with addition of boric acid. The enhanced polarization of nickel deposition in

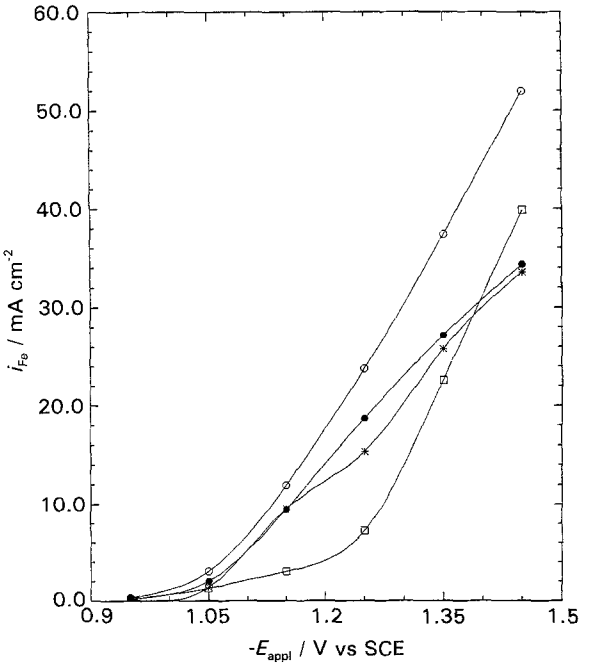

Fig. 13. Effect of various electrolytes on iron partial current density at $w = 3000$ rpm. Key as in Fig. 10.

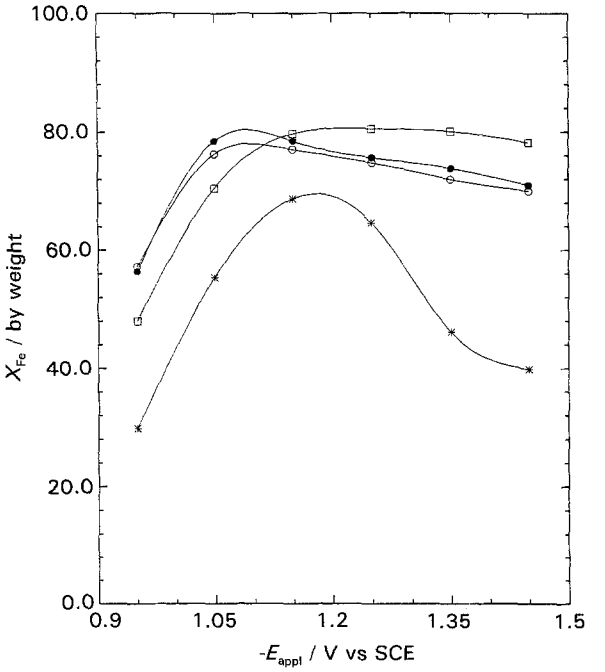

Fig. 15. Effect of different electrolytes on weight percentage of iron in the deposit. The deposition was carried out at $w = 3000$ rpm. Key as in Fig. 10.

the presence of boric acid seems to be associated with the blocking of the surface active sites by boric acid. Taking into account that a decrease in the reactive area due to the adsorption of an inactive species is a kinetic factor, in the presence of any surface agent on the surface, the rotation speed of the electrode should have a smaller influence on partial current densities. Figure 7 shows a smaller influence of electrode rotation speed on nickel partial current density when compared with Fig. 2. In contrast to nickel, the iron reaction rates shown in Fig. 8 increase in the presence of boric acid. Boric acid is used as a buffer agent in the traditional Watts electrolyte for bright nickel plating. However, according to Talbot's theoretical work [20] and the experimental work carried out by Horkans [21], boric acid has small buffer capacity in the electrolyte. Horkans also pointed out that boric acid may play a role as surface adsorption agent and this agrees with the results obtained in this study. As shown in Fig. 9, for each rotation of the electrode and for most of the potential range applied, the hydrogen partial current density in the bath containing boric acid is lower than the hydrogen partial current density obtained in the plain bath shown in Fig. 2. If boric acid has a significant buffer capacity, lower pH should be preserved at the interface, and as a consequence, the hydrogen partial current density should increase in the presence of boric acid. This phenomenon was not observed in Fig. 9. Further addition of ethylene diamine (EDA) or saccharin in the bath containing boric acid in Fig. 10 shows only a secondary inhibition. Compared with boric acid, EDA and saccharin have relatively less influence on the nickel partial current density against overvoltage dependence. Similar results in Fig. 11 were obtained for higher rotation rates. Overall, smaller nickel partial current densities were observed at higher rpms for all baths. Thus, the role of mass transfer can also be equally applied for more complicated solutions. As shown in Figs 12 and 13, the iron reaction rates increase in the presence of boric acid. Probably, the competition of $Ni(OH)^{+}_{ads}$ and $Fe(OH)^{+}_{ads}$ for surface sites is controlled by the presence of adsorbed boric acid. The adsorbed boric acid reduces the

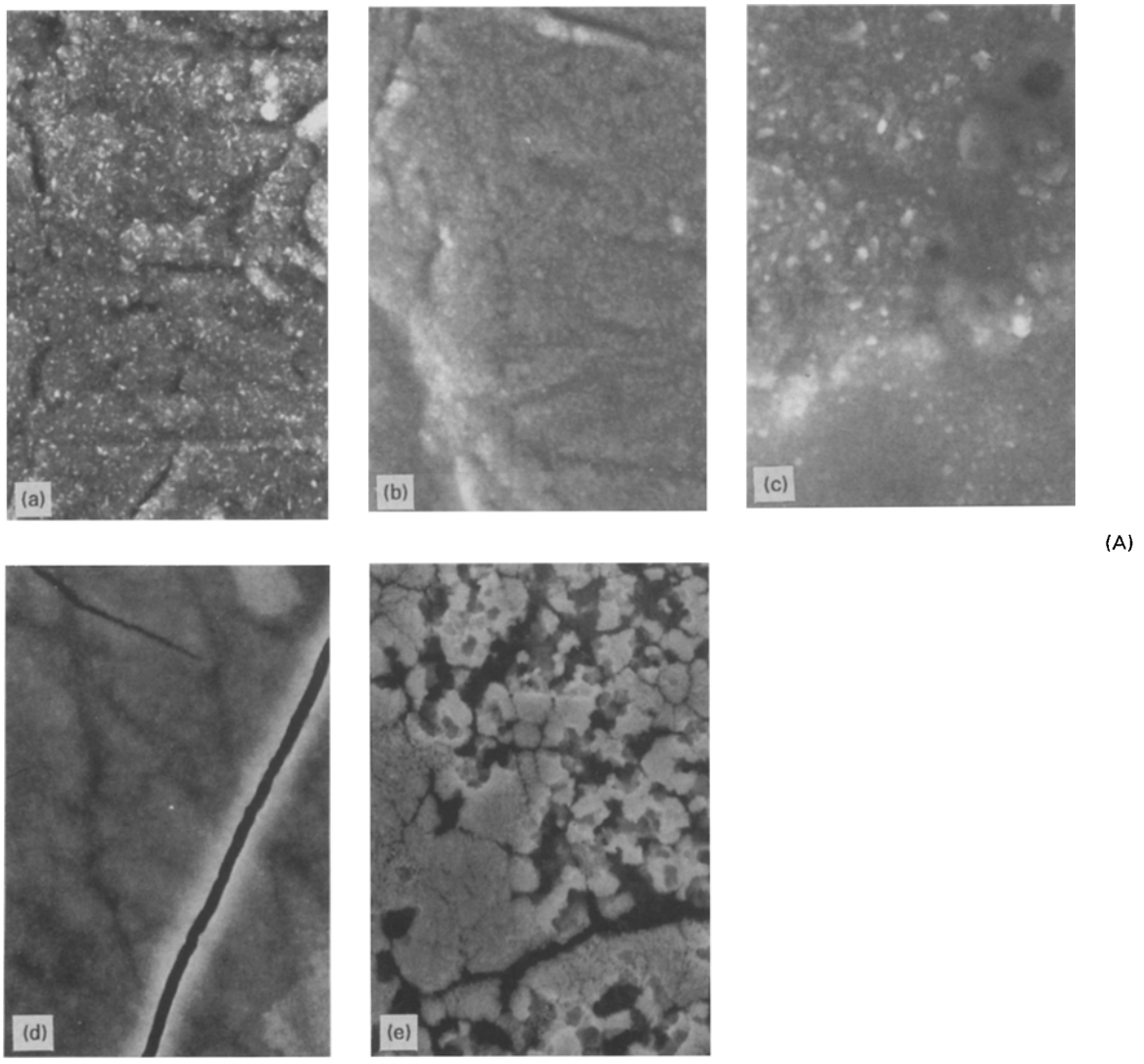

Fig. 16. SEMs of alloys deposited at different applied potentials from bath A containing: 0.5 M $NiSO_4$, 0.1 M $FeSO_4$, 0.5 M Na_2SO_4, pH 3. Overpotentials, E_{appl} (a) −0.9, (b) −1.0, (c) −1.075, (d) −1.2(centre) and (e) −1.2 V vs (SCE) (edge). Bath B containing: 0.5 M $NiSO_4$, 0.1 M $FeSO_4$, 0.5 M Na_2SO_4, 0.4 M boric acid and 0.01 M sodium saccharin, pH 3. Overpotentials: E_{appl} (a) −0.9, (b) −1.0, (c) = 1.075, (d) −1.2, (e) −1.4(centre) and (f): −1.4 V vs SCE(edge).

$Ni(OH)^+$ surface coverage, while allowing $Fe(OH)^+$ to be more highly incorporated on the surface. Bard and Faulkner [16] also discussed the possibility that the adsorbed materials may promote certain electrode reactions.

Similar to the plain bath, electrolytes containing organic additives always have higher iron partial current density as electrode rotation speed increases. It seems that EDA and saccharin play more important roles with the iron partial current density. As shown in Fig. 12 in the presence of EDA, the iron partial current density is significantly inhibited. EDA counteracts the positive effect of boric acid on iron deposition. The iron polarization in Fig. 12 is larger when compared with the plain bath in Fig. 4. In the presence of saccharin, the iron partial current density is more polarized at low overvoltages. In the high overpotential region, in the presence of saccharin, the iron partial current density increases faster when compared with the bath with no additives or with the bath containing boric acid and EDA. As a consequence, intersections of i_{Fe} curves are observed in Fig. 12. As shown in Fig. 13, a similar behaviour of the iron partial current density was found at 3000 rpm.

Different mechanisms are responsible for inhibition of the alloy deposition when carried out in the presence of EDA and saccharin. EDA is a known complexing agent for nickel and ferrous ions [22]. In the presence of EDA, Ni^{2+}-EDA and Fe^{2+}-EDA are formed, which decrease the concentration of free metal ions and metal hydroxyl ions in the electrolyte [22]. As a consequence, lower metal reduction rates are expected. In this case the interaction between the additive and the electroactive species occurs in the solution phase and is not a strong function of the applied potential.

On the other hand saccharin plays a role as a surfactant. Because of its surface blocking ability, the effective area for metal reaction is decreased. The coverage of the additive is expected to be larger at low overvoltages and smaller in the high overvoltage region [23, 24]. The decrease of the coverage by the additive at high applied potentials is probably due to the high inclusion rate of the additive under such conditions [25].

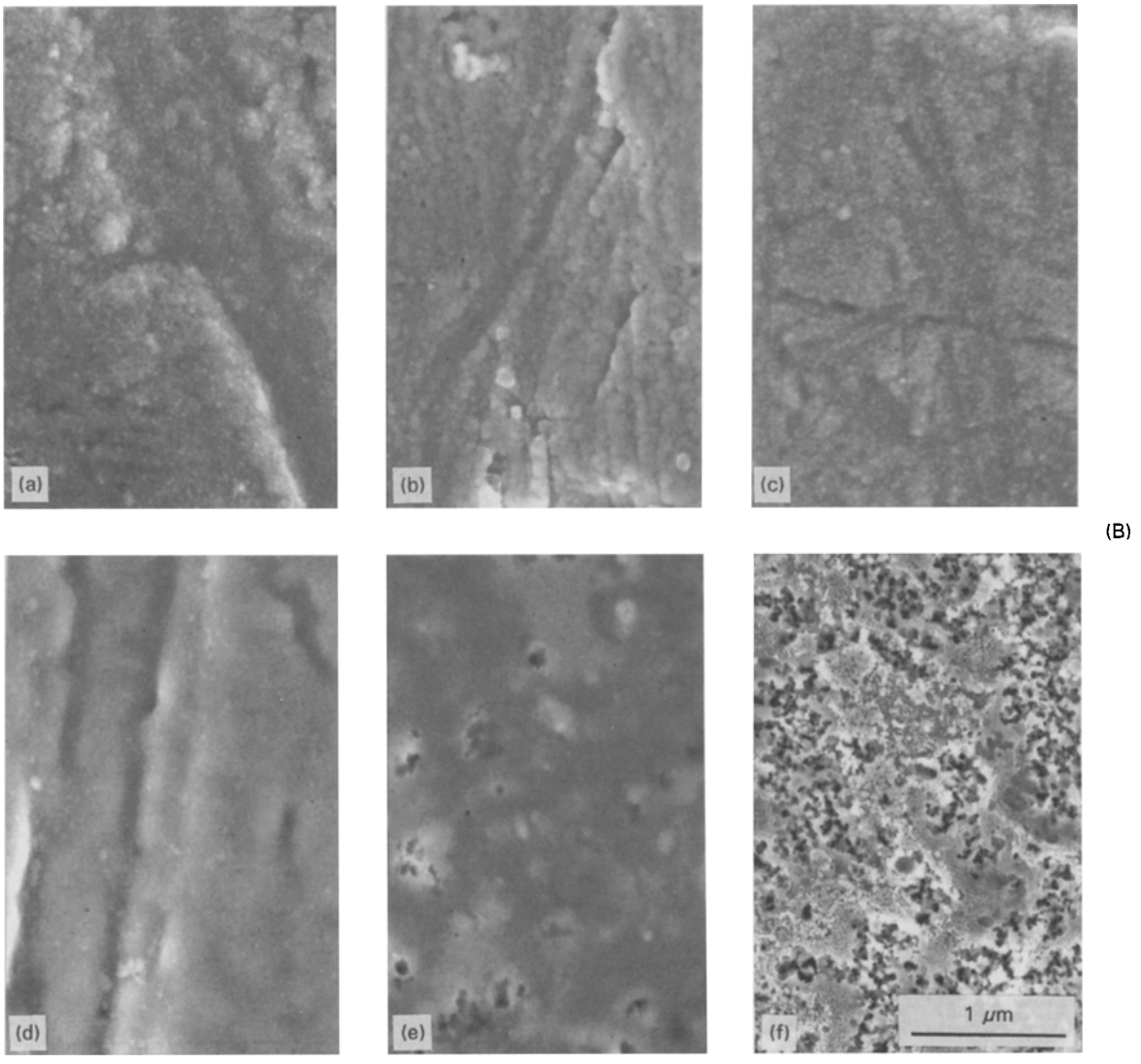

Fig. 16. Continued.

The composition indicated in Figs 14 and 15 are direct consequences of the iron and nickel deposition rates. At low rotation rates boric acid increases the iron percentage in the deposit significantly; while introduction of EDA and saccharin have smaller effects. A similar behaviour for the iron percentage is observed at 3000 rpm in Fig. 15, except that the decrease in the iron content after the maximum is smaller at high electrode rotation, indicating a positive effect of rotation speed on iron content at higher potential.

3.3. *Surface analysis*

To study the influence of the organic additives on the morphology of the electrodeposited Fe–Ni alloy, investigations were carried out using SEM. Fe–Ni alloys were plated potentiostatically with and without addition of boric acid and saccharin to the plating bath (0.5 M $NiSO_4$ + 0.1 M $FeSO_4$ + 0.5 M Na_2SO_4). Figure 16 shows micrographs for alloy films deposited at −0.9, −1.0, −1.075, −1.2 and at −1.4 V vs SCE. In the absence of organic additives,

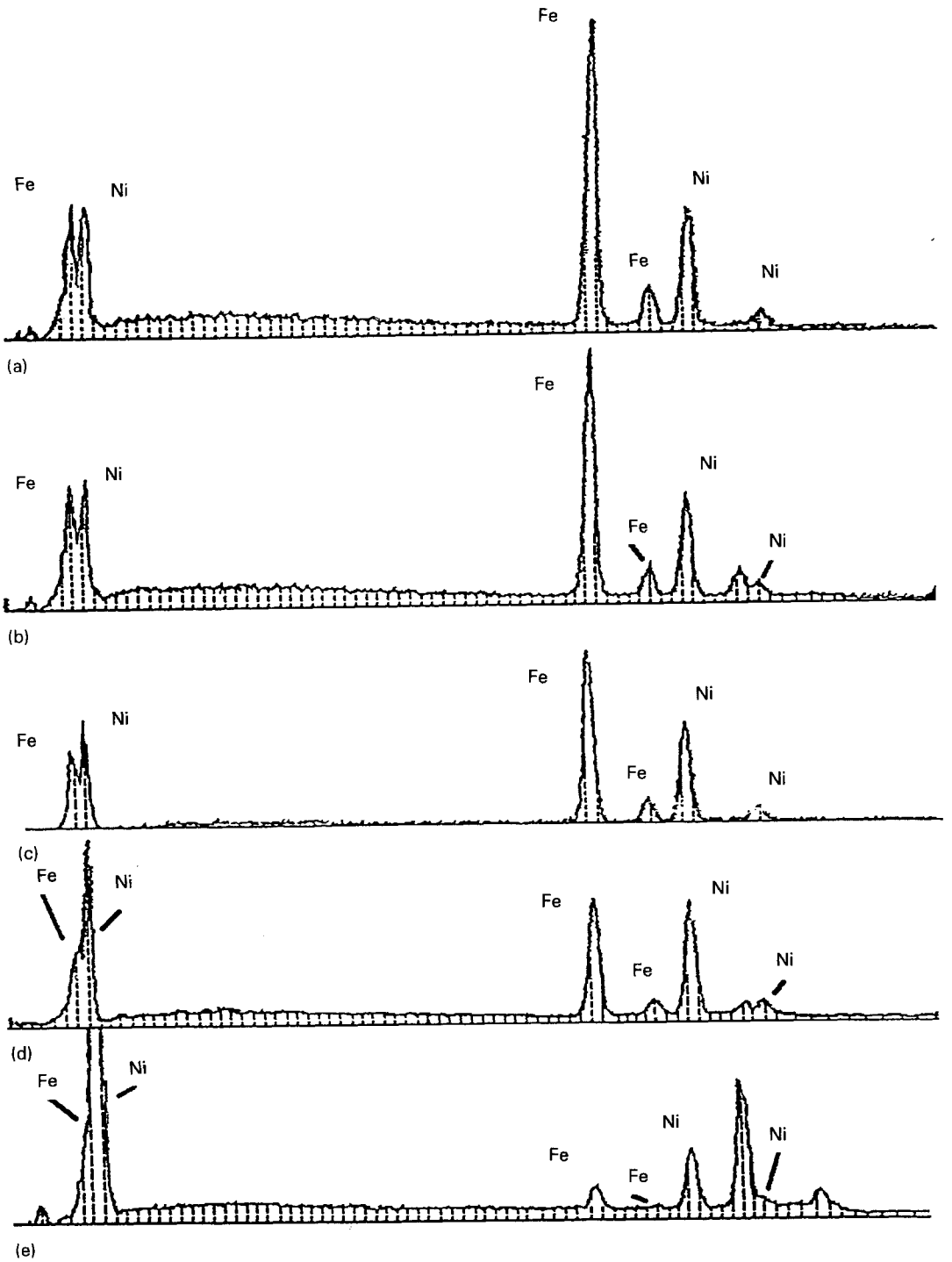

Fig. 17. Comparison of EDS spectrum obtained at different overpotentials in bath B; E_{appl}: (a) −1.4, (b) −1.2, (c) −1.075, (d) −1.0 and (e) −0.9 V vs SCE.

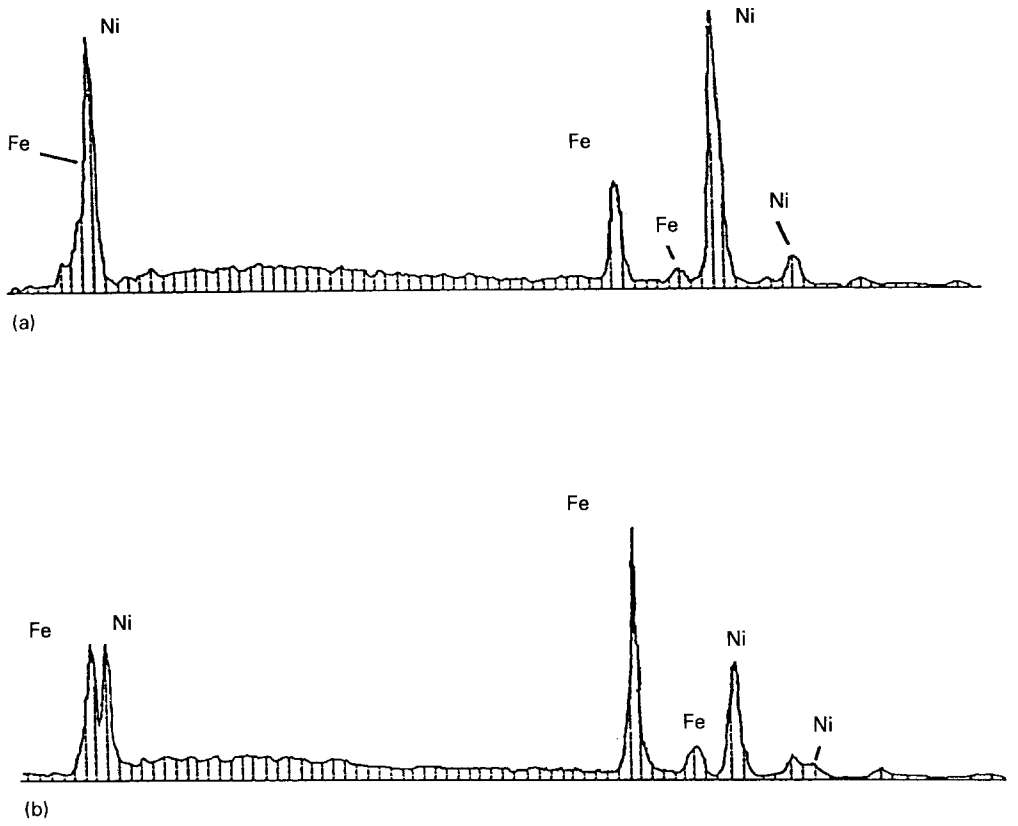

Fig. 18. EDS spectrum taken at $E_{appl} = -1.2$ V vs SCE in bath B, pH 3, at the edge of the plate (a), and at the centre of the plate (b).

cracks and black deposits appear at the corners and at the edges of the electrode, even at applied potential of −1.0 V vs SCE. The SEMs at the black edges in Fig. 16 show a porous structure. This phenomenon can be explained taking into account that higher overvoltage (higher current density) at the edges causes insufficient mass transfer of reactants and as a consequence a rise in the pH occurs, which induces a porous precipitation of $Ni(OH)_2$ and $Fe(OH)_2$. Cracking is caused by the relaxation of metal hydrides which are formed along with the hydrogen evolution reaction [26]. As seen in Fig. 16, the leveling effect is evident for deposits plated from the bath containing organic additives. The thin films deposited appear compact, homogeneous, adherent and very smooth. In the presence of organic additives, the occurrence of the burned area and precipitation of green $Ni(OH)_2$ was delayed to higher overpotentials. With addition of boric acid and saccharin, porous deposits were not observed up to −1.4 V vs SCE. The less effective exchange current density, due to the fractional coverage of the electrode by organic compounds, allows the concentration overvoltage to be reduced and surface overpotential to increase. As shown in this study, in the presence of organic compounds, the operating potential range is further extended, causing the proton concentration depletion to decrease significantly. As a consequence, as shown in Fig. 16, the occurrence of $Ni(OH)_2$ precipitation and porous structure shifts to the cathodic region indicating that the mass transfer limitation is delayed.

Figure 17 represents a comparison of EDS spectra at the centre of the plate obtained at different overpotentials. At low overpotential, the iron peak increases with increase in applied potential and levels off at higher overpotentials. In this region, the main electrode reactions yield nickel deposition and hydrogen evolution. In other words, at low overpotential, iron deposition is under kinetic control and by increasing the cathodic polarization, the Fe deposition rate is enhanced. Mass transfer limitation becomes more significant at higher overpotentials where, according to Fig. 14, the observed increase in iron content with the applied potential levels off and then decreases.

Figure 18 shows EDS spectra obtained at the edge and in the centre of plates deposited at −1.2 V vs SCE. The higher overpotential on the edge results in a high hydrogen evolution rate. As a consequence, rise of pH at the edges occurs which induces a porous precipitation of nickel and iron hydroxides. An average of 0.25 to 0.35 of Fe mole fraction was observed at the edges of the electrode compared with the values of 0.45 to 0.60 mole fractions of Fe observed at the centre of the plate. These results were not consistent with the Dahms and Croll mechanism [2, 3]. According to these authors a much higher Fe content would be expected on the edges, where higher current density and higher h.e.r. occur. As seen in Fig. 18 a clear oxygen peak occurred simultaneously with the nickel peaks at the edges, indicating the existence of $Ni(OH)_2$ rather than $Fe(OH)_2$. More $Ni(OH)_2$ precipitates on the

electrode at higher overpotentials. As reported in this study, the increased pH did not favour the iron deposition rate. According to the solution chemistry of Fe–Ni plating baths presented in Fig. 1, $Ni(OH)_2$ should be precipitated preferentially to $Fe(OH)_2$.

4. Conclusion

The codeposition of Fe–Ni alloys in the presence of organic additives is explained taking into account Fe–Ni plating bath solution chemistry, mass transfer of ionic species, surface adsorption effects and electrode surface reactions. The concentrations of all electroactive species in the bath were calculated by using various element balances, equilibrium conditions, and the electroneutrality condition for a specified pH. Because of the difference in metal hydroxide ion stability constants, $Ni(OH)_2$ precipitation occurs at a pH two units smaller than $Fe(OH)_2$. Besides the fact that Ni^{2+} ions are present in the electrolyte in much higher concentration than Fe^{2+}, the $Fe(OH)^+$ concentration is two orders of magnitude larger than $Ni(OH)^+$ concentration. Also, Fe^{2+} and $Fe(OH)^+$ ions have a larger buffer capacity than Ni^{2+} and $Ni(OH)^+$ ions. The adsorbed $Fe(OH)^+$ reduces the active sites for $Ni(OH)^+$ adsorption and, consequently, inhibits the nickel reduction rate. However, it was found that the ferrous ion can also stabilize the nickel ion from precipitation. The iron composition profiles were explained taking into account the kinetic parameters of both electrodeposition processes. The alloy compositions were determined by the competition of reactive species on the electrode surface. The role of the additives on Fe–Ni codeposition was explained by the effect of surface coverage or solution complexation.

Acknowledgements

The first author appreciates the assistance of Prof. S. H. Lin for acquiring certain research instruments. Technical assistance by S. F. Chiang, C. L. Lee and S. L. Fan is gratefully acknowledged. This work was supported by the People's Republic of China National Science Council (NSC 82-0113-E-155-077-T), Sandia National Laboratories, and AESF projects RF-83.

References

[1] I. M. Croll and L. T. Romakiw, *in* Proceedings of the Symposium on Electrodeposition Technology, Theory and Practice (edited by L. T. Romankiw), The Electrochemical Society Softbound Series, PV87-17, Pennington, NJ (1987).
[2] H. Dahms, *J. Electroanal. Chem. Interfacial Electrochem.* **8** (1964) 5.
[3] H. Dahms and I. M. Croll, *J. Electrochem. Soc.* **112** (1965) 771.
[4] L. T. Romankiw, *in* Proceedings of the Symposium on Electrodeposition Technology, Theory and Practice (edited by L. T. Romankiw), The Electrochemical Society Softbound Series, PV87-17, Pennington, NJ (1987).
[5] M. J. Nichol and H. I. Philip, *J. Electroanal. Chem. Interfacial Electrochem.* **70** (1976) 233.
[6] P. C. Andricacos, C. Arana, J. Tabib, J. Dukovic and Romankiw, *J. Electrochem. Soc.* **136** (1989) 1336.
[7] P. C. Andricacos, J. Tabib and L. T. Romankiw, *ibid.* **135** (1988) 1172.
[8] W. C. Grande and J. B. Talbot, *ibid.* **136** (1989) 3611.
[9] D. Gangasingh and J. B. Talbot, *ibid.* **138** (1991) 3605.
[10] S. Hessami and C. W. Tobias, *ibid.* **136** (1989) 3611.
[11] J. O'M. Bockris, D. Drazic and A. R. Despic, *Electrochim. Acta* **4** (1961) 325.
[12] J. Matulis and R. Slizys, *ibid* **9** (1964) 1177.
[13] M. Matlosz, *J. Electrochem.Soc.* **140** (1993) 2272.
[14] B. N. Popov, S. N. Popova, K.-M. Yin and R. E. White, *Plat. Surf. Finish* **81** (1994) 65.
[15] B. N. Popov, K.-M. Yin and R. E. White, *J. Electrochem. Soc.* **140** (1993) 1321.
[16] A. J. Bard and L. R. Faulkner, 'Electrochemical Methods: Fundamentals and Applications', John Wiley & Sons (1980) pp. 538–9.
[17] J. Horkans, *J. Electrochem. Soc.* **128** (1981) 45.
[18] N. Nakamura and T. Hayashi, *Plat. Surf. Finish.* **72** (1985) 42.
[19] N. Tanaka and R. Tamamushi, *Electrochim. Acta* **9** (1964) 963.
[20] W. C. Grande and Talbot, *J. Electrochem. Soc.* **140** (1993) 675.
[21] J. Horkans, *ibid.* **126** (1979) 1861.
[22] S. N. Srimathi and S. M. Mayanna, *J. Appl. Electrochem.* **13** (1983) 679.
[23] S. Roy and P. N. Pintauro, *J. Electrochem. Soc.* **140** (1993) 3167.
[24] L. K. Patridge, A. C. Tansley and Porter, *Electrochim. Acta* **11** (1966) 517.
[25] D. Roha and U. Landau, *J. Electrochem. Soc.* **137** (1990) 824.
[26] N. Hackerman and T. Jensen, *ibid.* **99** (1952) 60.

Appendix

For region I the variables to be determined are $[Fe^{2+}]$, $[Fe(OH)^+]$, $[Ni^{2+}]$, $[Ni(OH)^+]$, $[OH^-]$, $[H_2O]$, $[HSO_4^-]$, $[SO_4^{2-}]$, and $[H_2SO_4]_{ad}$ or $[NaOH]_{ad}$, depending on the specified pH. The equations needed are: (a) the element balance on oxygen,

$$[H_2O]_{ad} + 4[Na_2SO_4]_{ad} + 4[FeSO_4]_{ad} + 4[NiSO_4]_{ad} + 4[H_2SO_4]_{ad} = [OH^-] + [Fe(OH)^+] + [Ni(OH)^+] + [H_2O] + 4[HSO_4^-] + 4[SO_4^{2-}] \quad (11)$$

(b) the element balance on sulfur,

$$[Na_2SO_4]_{ad} + [FeSO_4]_{ad} + [NiSO_4]_{ad} + [H_2SO_4]_{ad} = [HSO_4^-] + [SO_4^{2-}] \quad (12)$$

(c) the element balance on iron,

$$[FeSO_4]_{ad} = [Fe^{2+}] + [Fe(OH)^+] \quad (13)$$

(d) the element balance on nickel,

$$[NiSO_4]_{ad} = [Ni^{2+}] + [Ni(OH)^+] \quad (14)$$

(e) the electroneutrality,

$$2[Na_2SO_4]_{ad} + [H^+] + 2[Fe^{2+}] + 2[Ni^{2+}] + [Fe(OH)^+] + [Ni(OH)^+] = [OH^-] + [HSO_4^-] + 2[SO_4^{2-}] \quad (15)$$

(f) the equilibrium conditions,

$$[H^+][SO_4^{2-}] - K_1[HSO_4^-] = 0 \quad (16)$$

$$[Ni^{2+}][OH^-] - K_2[Ni(OH)^+] = 0 \quad (17)$$

$$[Fe^{2+}][OH^-] - K_3[Fe(OH)^+] = 0 \quad (18)$$

$$[H^+][OH^-] - K_4 = 0 \quad (19)$$

Note the element balance of hydrogen is not independent, because it can be derived by algebraic manipulations of the other balances. Depending on the pH value specified, either the variable $[H_2SO_4]_{ad}$ or the variable $[NaOH]_{ad}$ can be determined.

For region II the variables that must be determined are $[Fe^{2+}]$, $[Fe(OH)^+]$, $[Ni^{2+}]$, $[Ni(OH)^+]$, $[OH^-]$, $[H_2O]$, $[HSO_4^-]$, $[SO_4^{2-}]$, $[Ni(OH)_2(s)]$ and $[NaOH]_{ad}$. Note that $[Ni(OH)_2(s)]$ is based on one litre volume of solutions. The equations are

(a) the element balance on oxygen,

$$[H_2O]_{ad} + 4[Na_2SO_4]_{ad} + 4[FeSO_4]_{ad} + 4[NiSO_4]_{ad} + [NaOH]_{ad} = [OH^-] + [Fe(OH)^+] + [Ni(OH)^+] + [H_2O] + 4[HSO_4^-] + 4[SO_4^{2-}] + 2[Ni(OH)_2(s)] \quad (20)$$

(b) the element balance on sulfur,

$$[Na_2SO_4]_{ad} + [FeSO_4]_{ad} + [NiSO_4]_{ad} = [HSO_4^-] + [SO_4^{2-}] \quad (21)$$

(c) the element balance on iron (Equation 13)

(d) the element balance on nickel,

$$[NiSO_4]_{ad} = [Ni^{2+}] + [Ni(OH)^+] + [Ni(OH)_2(s)] \quad (22)$$

(e) the electroneutrality condition,

$$2[Na_2SO_4]_{ad} + [NaOH]_{ad} + [H^+] + 2[Fe^{2+}] + 2[Ni^{2+}] + [Fe(OH)^+] + [Ni(OH)^+] = [OH^-] + [HSO_4^-] + 2[SO_4^{2-}] \quad (23)$$

(f) the equilibrium conditions: Equations 16, 17, 18, 19 and

$$[Ni(OH)^+][OH^-] - K_{d,Ni(OH)_2} = 0 \quad (24)$$

For region III the variables to be determined are $[Fe^{2+}]$, $[Fe(OH)^+]$, $[Ni^{2+}]$, $[Ni(OH)^+]$, $[OH^-]$, $[H_2O]$, $[HSO_4^-]$, $[SO_4^{2-}]$, $[Ni(OH)_2(s)]$, $[Fe(OH)_2(s)]$, and $[NaOH]_{ad}$. The Equations are

(a) the element balance on oxygen,

$$[H_2O]_{ad} + 4[Na_2SO_4]_{ad} + 4[FeSO_4]_{ad} + 4[NiSO_4]_{ad} + [NaOH]_{ad} = [OH^-] + [Fe(OH)^+] + [Ni(OH)^+] + [H_2O] + 4[HSO_4^-] + 4[SO_4^{2-}] + 2[Ni(OH)_2(s)] + 2[Fe(OH)_2(s)] \quad (25)$$

(b) the element balance on sulfur: Equation 21.

(c) the element balance on iron

$$[FeSO_4]_{ad} = [Fe^{2+}] + [Fe(OH)^+] + [Fe(OH)_2(s)] \quad (26)$$

(d) the element balance on nickel: Equation 22.

(e) the electroneutrality condition: Equation 23.

(f) the equilibrium conditions: Equations 16–19 and 24 and

$$[Fe(OH)^+][OH^-] - K_{d,Fe(OH)_2} = 0 \quad (27)$$

These equations were solved by using the Newton–Raphson iterative method.